Comparison of Aqueous Molecular Dynamics with NMR Relaxation and Residual Dipolar Couplings Favors Internal Motion in a Mannose Oligosaccharide

Andrew Almond,*,† Jakob Bunkenborg,‡ Thomas Franch,§ Charlotte H. Gotfredsen,† and Jens Ø. Duus†

Contribution from the Carlsberg Laboratory, Gamle Carlsberg Vej 10, Valby, Copenhagen DK 2500, Denmark, Department of Chemistry, University of Southern Denmark, Odense University, Odense DK 5230, Denmark, and Department of Molecular Biology, University of Southern Denmark, Odense University, Odense DK 5230, Denmark

Received July 13, 2000. Revised Manuscript Received February 6, 2001

Abstract: An investigation has been performed to assess how aqueous dynamical simulations of flexible molecules can be compared against NMR data. The methodology compares state-of-the-art NMR data (residual dipolar coupling, NOESY, and ^{13}C relaxation) to molecular dynamics simulations in water over several nanoseconds. In contrast to many previous applications of residual dipolar coupling in structure investigations of biomolecules, the approach described here uses molecular dynamics simulations to provide a dynamic representation of the molecule. A mannose pentasaccharide, α-D-Man*p*-(1→3)-α-D-Man*p*-(1→3)-α-D-Man*p*-(1→3)-α-D-Man*p*-(1→2)-D-Man*p*, was chosen as the model compound for this study. The presence of α-linked mannan is common to many glycopeptides, and therefore an understanding of the structure and the dynamics of this molecule is of both chemical and biological importance. This paper sets out to address the following questions. (1) Are the single structures which have been used to interpret residual dipolar couplings a useful representation of this molecule? (2) If dynamic flexibility is included in a representation of the molecule, can relaxation and residual dipolar coupling data then be simultaneously satisfied? (3) Do aqueous molecular dynamics simulations provide a reasonable representation of the dynamics present in the molecule and its interaction with water? In summary, two aqueous molecular dynamics simulations, each of 20 ns, were computed. They were started from two distant conformations and both converged to one flexible ensemble. The measured residual dipolar couplings were in agreement with predictions made by averaging the whole ensemble and from a specific single structure selected from the ensemble. However, the inclusion of internal motion was necessary to rationalize the relaxation data. Therefore, it is proposed that although residual dipolar couplings can be interpreted as a single-structure, this may not be a correct interpretation of molecular conformation in light of other experimental data. Second, the methodology described here shows that the ensembles from aqueous molecular dynamics can be effectively tested against experimental data sets. In the simulation, significant conformational motion was observed at each of the linkages, and no evidence for intramolecular hydrogen bonds at either α(1→2) or α(1→3) linkages was found. This is in contrast to simulations of other linkages, such as *β*(1→4), which are often predicted to maintain intramolecular hydrogen bonds and are coincidentally predicted to have less conformational freedom in solution.

Introduction

Complex carbohydrates play key roles in biological recognition processes[1,2] and in the progression of disease.[3] Although their function and the detailed mechanisms of their biological action are poorly understood, their activity is proposed to be dependent on shape and dynamics.[4] Therefore, if the importance of these molecules to biology and medicine is to be fully realized, an appreciation of their physical behavior at the molecular level is crucial.[5,6] If it is assumed that biomolecular shape and dynamic behavior result from the dynamical interaction with surrounding water molecules,[7] then it is possible that computer simulations which include explicit water can provide this information.[8] Recent advances in computer power now allow extensive simulations which include molecular water to be performed. Subsequently, these simulations can be compared directly with experimental data. It is proposed that when computer simulations can be effectively tested against experimental data, they can be used to provide detailed microscopic information which is of biological relevance. Here we extend previous work, which successfully compared aqueous molecular

† Carlsberg Laboratory.
‡ Department of Chemistry, University of Southern Denmark.
§ Department of Molecular Biology, University of Southern Denmark.

(1) Peters, T.; Pinto, B. M. *Curr. Opin. Struct. Biol.* **1996**, *6*, 710−720.
(2) Rudd, P. M.; Dwek, R. A. *Crit. Rev. Biochem. Mol. Biol.* **1997**, *32*, 1−100.
(3) Rudd, P. M.; Endo, T.; Colominas, C.; Groth, D.; Wheeler, S. F.; Harvey, D. J.; Wormald, M. R.; Serban, H.; Prusiner, S. B.; Kobata, A.; Dwek, R. A. *Proc. Nat. Acad. Sci. U.S.A.* **1999**, *96*, 13044−13049.
(4) Dwek, R. A. *Chem. Rev.* **1996**, *96*, 683−720.
(5) Bush, C. A.; Martin-Pastor, M.; Imberty, A. *Annu. Rev. Biophys. Biomol. Struct.* **1999**, *28*, 269−293.
(6) Imberty, A.; Pérez, S. *Chem. Rev.* **2000**, *100*, 4567−4588.
(7) Vishnyakov, A.; Widmalm, G.; Laaksonen, A. *Angew. Chem., Int. Ed.* **2000**, *39*, 140−142.
(8) Liu, Q.; Brady, J. W. *J. Am. Chem. Soc.* **1996**, *118*, 12276−12286.

10.1021/ja0025696 CCC: $20.00
Published on Web 04/27/2001

dynamics simulations against X-ray fiber diffraction and hydrodynamic measurements.[9−11]

In NMR investigations, relaxation is commonly used to sense fast internal motions,[12] whereas residual dipolar couplings are used to provide global structural information.[13] These techniques therefore provide complementary information about structure and dynamics and together are a demanding test of the dynamic data resultant from simulations. The methodology used here tests molecular dynamics over several nanoseconds against state-of-the-art nuclear magnetic resonance (NMR) methods. Using this approach, the following fundamental questions were addressed for an oligosaccharide. First, single structures have frequently been used to interpret residual dipolar couplings, but is this a useful representation of a flexible molecule? Second, when dynamic flexibility is included in a representation of the molecule, can NMR relaxation and residual dipolar coupling data be simultaneously satisfied? Finally, do aqueous molecular dynamics simulations provide a reasonable representation of the dynamics present in the molecule and its interaction with water?

A mannose pentasaccharide, containing both α(1→2) and α(1→3) linkages (Figure 1), was chosen as a model system for testing our methodology. Along with the presence of α-linked mannose in polysaccharides, many glycoproteins contain this type of sugar unit and linkage.[2,14] Therefore, an understanding of the structure and dynamics of α-linked mannose is of both chemical and biological importance. The pentamannan used here is the most abundant repeating unit in the side chains of the extracellular phospho-mannan produced by the yeast species *Pichia (Hansenula) holstii* NRRL Y-2448.[15]

Oligosaccharides containing α-linked mannose residues have previously been studied by molecular modeling in both vacuum[16] and water.[17] Modeling studies have also been combined with NMR relaxation,[18,19] optical rotation,[20] and X-ray crystallography data.[21] The results from these studies indicate that a predominant conformation exists for both the α(1→2) and the α(1→3) linkages, but minor populations of other conformers could not be ruled out on the basis of the experimental data used. However, in none of these studies has molecular modeling been simultaneously tested against NMR relaxation and an experimental technique capable of providing detailed information on global conformation, such as residual dipolar coupling measurement.[22]

Filamentous phages[23] were used to induce orientational anisotropy in an oligosaccharide cosolute and allow the measurement of residual dipolar couplings by NMR techniques. For directly bonded nuclei (e.g., C−H), the residual dipolar couplings contain valuable information on the orientation of internuclear vectors relative to the magnetic field. Each bond vector can be related to a molecule-fixed principal coordinate system describing the molecular alignment with respect to the magnetic field, and thereby give global angular information. A spin-state-selective (S^3) technique[24,25] was used to measure residual dipolar couplings, which offers a convenient and accurate method for measuring coupling constants by editing the α and β S spin states of the IS two spin system into different

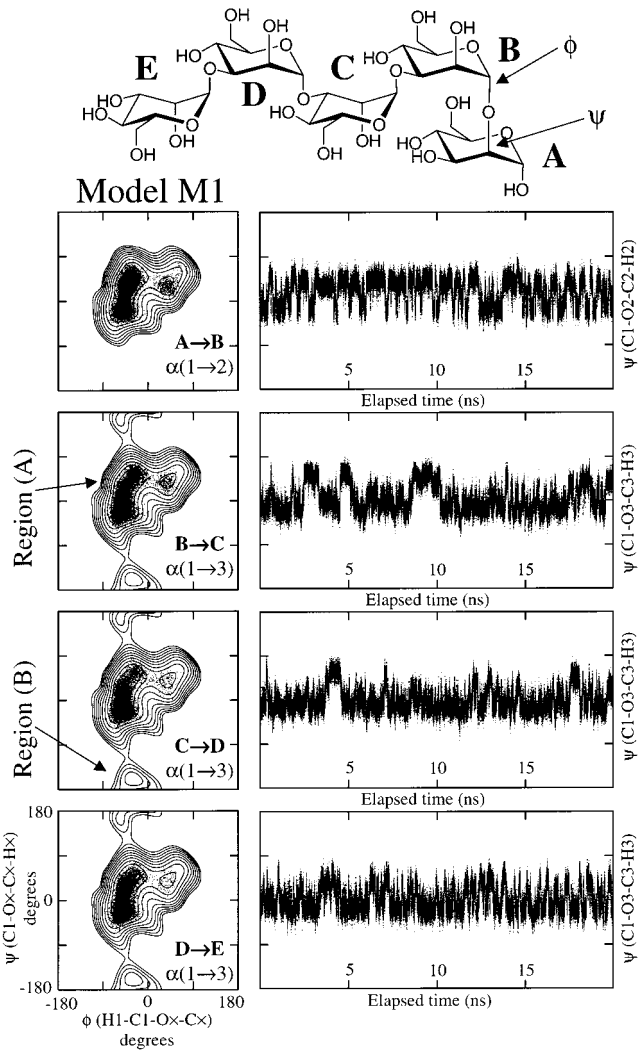

Figure 1. The chemical structure of the pentamannan oligosaccharide, showing the labeling of the sugar residues (A−E) (top). Exploration of the glycosidic linkages during a 20 ns simulation where all of the α(1→3) linkages were started in low-energy conformational region (A), which is labeled on the figure. To the left scatter diagrams are plotted, showing all (ϕ,ψ) angles explored during the simulation for all four linkages of the pentamannan. The position of each linkage in the structure is specified in the lower right of each diagram. Under the scattered points, a contour diagram showing the estimated vacuum molecular energy surface is plotted for the lowest energies (see Materials and Methods). To the right the exploration of the ψ angles during the simulation are plotted, and it is noticed that no transitions were observed between the two low-energy regions (A) and (B). The ensemble created by this simulation represents dynamic model M1.

(9) Almond, A.; Brass, A.; Sheehan, J. K. *J. Mol. Biol.* **1998**, *284*, 1425−1437.
(10) Almond, A.; Sheehan, J. K. *Glycobiology* **2000**, *10*, 329−338.
(11) Almond, A.; Brass, A.; Sheehan, J. K. *J. Phys. Chem. B* **2000**, *104*, 5634−5640.
(12) Widmalm, G. Physical methods in carbohydrate research. In *Carbohydrate Chemistry*; Boons, G. J., Ed.; Blackie Academic & Professional: London, 1998; pp 448−502.
(13) Tjandra, N.; Bax, A. *Science* **1997**, *278*, 1111−1114.
(14) Lis, H.; Sharon, N. *Eur. J. Biochem.* **1993**, *218*, 1−27.
(15) Parolis, L. A. S.; Parolis, H.; Kenne, L.; Meldal, M.; Bock, K. *Carbohydr. Res.* **1998**, *309*, 77−87.
(16) Balaji, P. V.; Qasba, P. K.; Rao, V. S. R. *Glycobiology* **1994**, *4*, 497−515.
(17) Edge, C. J.; Singh, U. C.; Bazzo, R.; Taylor, G. L.; Dwek, R. A.; Rademacher, T. W. *Biochemistry* **1990**, *29*, 1971−1974.
(18) Rutherford, T. J.; Homans, S. W. *Biochemistry* **1994**, *33*, 9606−9614.
(19) Woods, R. J.; Pathiaseril, A.; Wormald, M. R.; Edge, C. J.; Dwek, R. A. *Eur. J. Biochem.* **1998**, *258*, 372−386.
(20) Stevens, E. S. *Biopolymers* **1994**, *34*, 1395−1401.
(21) Homans, S. W. *Biochemistry* **1990**, *29*, 9110−9118.
(22) Losonczi, J. A.; Andrec, M.; Fischer, M. W. F.; Prestegard, J. H. *J. Magn. Reson.* **1999**, *138*, 334−342.
(23) Hansen, M. R.; Mueller, L.; Pardi, A. *Nat. Struct. Biol.* **1998**, *5*, 1065−1074.
(24) Meissner, A.; Duus, J. Ø.; Sørensen, O. W. *J. Biomol. NMR* **1997**, *10*, 89−94.
(25) Meissner, A.; Duus, J. Ø.; Sørensen, O. W. *J. Magn. Reson.* **1997**, *128*, 92−97.

Table 1. ^{1}H Chemical Shift Assignments for the Mannan Pentasaccharide[a]

residue (Figure 1)	measmt	H1	H2	H3	H4	H5	H6a,b
A	δ (ppm)	5.380	3.961	3.951	3.703	3.807	3.876/3.764
	T_1 (s)	2.2/2.4	1.7/1.9	1.7/1.9	2.6/2.8		
	T_2 (s)	0.7/0.2			0.2/0.4		
B	δ (ppm)	5.038	4.232	3.964	3.757	3.803	3.882/3.749
	T_1 (s)	2.0/2.2	1.8/1.9	1.7/1.9			
	T_2 (s)	0.7/0.5	0.3/0.2				
C	δ (ppm)	5.130	4.232	4.018	3.765	3.835	3.911/3.762
	T_1 (s)	2.0/2.2	1.8/2.0	1.5/1.6			
	T_2 (s)	0.3/0.5	0.3/0.2				
D	δ (ppm)	5.120	4.237	4.025	3.763	3.844	3.917/3.762
	T_1 (s)	2.0/2.2	1.8/1.9	1.5/1.6			
	T_2 (s)	0.5/0.5	0.3/0.2				
E	δ (ppm)	5.141	4.078	3.889	3.644	3.797	3.915/3.751
	T_1 (s)	1.9/2.1	2.2/2.5	1.4/1.3	3.1/3.5		0.9/0.9
	T_2 (s)			0.3/0.3			0.3/0.2

[a] The residual labeling is evident in Figure 1. Also shown are the measured proton T_1 and T_2 values, where measurement was possible. These values were measured without and with phages present, and the two values are separated by a slash.

subspectra. The spin-state-selective coherence transfer (S^3CT) element[26] introduced for measuring scalar coupling constants in isotropic solution is also well suited for measurements of residual dipolar couplings in weakly aligning media. For measurement of one-bond $^{13}C-^1H$ residual dipolar couplings in natural abundance, a previously published pulse sequence was adapted,[27] which is only suitable for measuring CH and not CH_2 or CH_3 residual dipolar couplings. To obtain $^1H-^1H$ residual dipolar couplings, the S^3CT TOCSY experiment was used,[26] which yields both their sign and magnitude.

Materials and Methods

The pentamannose oligosaccharide was isolated in a previous study[15,28] by cleavage from a core phospho-mannan of *Pichia (Hansenula) holstii* NRRL Y-24448. After reassignment of the pentamannan chemical shifts at 800 MHz, a higher field than previously, the increased resolution revealed that the original assignment contained an error,[15] and hence it is necessary to report them again, Table 1. Pf1 filamentous phages were prepared and purified as previously described[23,29] and resuspended in a 10 mM phosphate D_2O buffer, giving a phage concentration of 22 mg/mL with a residual ^2H quadrupolar splitting of $\approx$16 Hz. To this, 5.6 mg of oligosaccharide was added to give a final sample volume of 600 μL.

All 2D S^3CT spectra for measurement of one-bond $^1H-^{13}C$ residual coupling constants, homonuclear NOESY and DQF-COSY spectra, ^1H T_1 and ^1H T_2 experiments were recorded on a Varian Unity Inova 800 MHz spectrometer. The 2D S^3CT TOCSY experiments for measurements of homonuclear $^1H-^1H$ residual dipolar couplings were recorded on a Varian Unity Inova 500 MHz spectrometer. The ^{13}C T_1 relaxation experiments were performed using a Bruker DRX 600 MHz spectrometer. Experiments were performed at a constant temperature of 298 K. All 2D spectra were processed with the Bruker XWINNMR software package (version 2.1). All simulations were performed on a dual processor Compaq Alpha workstation.

Measurement of NMR Relaxation Parameters. The ^1H T_1 experiments were acquired using a standard 1D inversion recovery experiment, with a 13 s delay between each scan and an acquisition time of 3 s. A total of 18 different T_1 relaxation periods were recorded in the range 0.01 to 10 s. The ^1H T_2 experiments were acquired using a standard Carr-Purcell-Meiboom-Gill experiment with a relaxation delay of 6 s, acquisition time of 2 s, and spin echo cycle time of 2 ms. A total of 32 different T_2 relaxation delays were used in the range 0.032 to 1.2 s. The ^1H T_1 and ^1H T_2 values for different protons were extracted using a three-parameter fit to the peak heights, by assuming an exponential decay of magnetization by the relaxation process. This is of course an approximation, which assumes that proton magnetization decays in an analogous way to a two-spin system.[30]

NOESY spectra were recorded with mixing times of 150, 300, and 450 ms. They were acquired with a relaxation delay of 2.7 s: 16 scans and 256 complex increments. The spectral width was 3000 Hz in both dimensions covered by a data-matrix of 512 $\times$ 2048 points. The spectra were zero-filled to 1024 $\times$ 2048 points and a squared sine (shifted by $\pi/3$) window function was applied.

A 2D INEPT inversion−recovery−HSQC experiment was designed to measure ^{13}C T_1 values. The sweep width was 2500 Hz $\times$ 7300 Hz, and the acquisition was 128 $\times$ 2048 points. This was zero-filled to 512 $\times$ 2048 points, and a cosine square window function was applied. A total of 12 spectra were recorded with relaxation times in the range 0.02 to 3.0 s. The spectra were recorded in a nonsystematic order of relaxation delays, and the total recycle time was maintained at 6 s. Intensities were obtained from the spectra by integrating resolved peaks. The T_1 values were calculated by assuming a single-exponential decay and using a three-parameter fit to the experimental intensities as a function of time.

Measurement of Residual Dipolar Couplings. The pulse sequences for measurement of residual dipolar couplings all utilized the S^3CT (spin-state-selective) element[31] to obtain a pair of two-dimensional spectra containing α and β spin states, respectively. The difference in splitting between α and β spin states in the absence and presence of phages was taken as the residual dipolar coupling. These were measured from 1D slices of the 2D spectra with an estimated error of $\pm$ 0.4 Hz. To measure heteronuclear couplings, a previously published sequence[27] based on gradient HSQC was adapted, and to measure homonuclear proton couplings a TOCSY-type experiment was used.[26] The S^3CT-HSQC parameters were relaxation delay 2.5 s, τ = 3.22 ms, δ = 1.1 ms, t_1(max) = 24 ms, and a total of 16 scans for each set of experiments. Spectral widths of 13000 Hz in ^{13}C and 2200 Hz in the ^1H were recorded in a data matrix of 626 $\times$ 4096 points. The sorting of the S^3CT spectral data into subspectra prior to processing was done using a C-program,[27] as described previously. The subspectra were zero-filled to 1024 $\times$ 4096 points, and cosine window functions were applied in both dimensions. The S^3CT-TOCSY parameters were relaxation delay 1.5 s, DIPSI-2 mixing time = 70 ms, t_1(max) = 64 ms, τ = 3.22 ms, 160 scans, and 128 t_1 increments. A spectral width of 2000 Hz was used in both dimensions and covered by a data matrix of 256 $\times$ 1024 points. The subspectra were zero-filled to 1024 $\times$ 8192 points and apodized with cosine window functions in both dimensions.

(26) Sørensen, M. D.; Meissner, A.; Sørensen, O. W. *J. Biomol. NMR* **1997**, *10*, 181−186.
(27) Lerche, M. H.; Meissner, A.; Poulsen, F. M.; Sørensen, O. W. *J. Magn. Reson.* **1999**, *140*, 259−263.
(28) Parolis, L. A. S.; Duus, J. Ø.; Parolis, H.; Meldal, M.; Bock, K. *Carbohydr. Res.* **1996**, *293*, 101−117.
(29) Hansen, M. R.; Hanson, P.; Pardi, A. *Methods Enymol.* **2000**, *317*, 220−240.
(30) Macura, S.; Ernst, R. R. *Mol. Phys.* **1980**, *41*, 95−117.
(31) Nielsen, N. C.; Thøgersen, H.; Sørensen, O. W. *J. Chem. Phys.* **1996**, *105*, 3962−3968.

Molecular Dynamics Simulations. Simulations were performed using the general molecular modeling package CHARMM.[32] The most current carbohydrate force-field parameters suitable for CHARMM were used, with inclusion of terms to effectively model the exo-anomeric effect.[33] A consistent set of partial charges for a mannose sugar in the $^4C_1$ configuration was obtained using a 6-31g Hartree−Fock basis set *ab initio* calculation. Each structure was initially relaxed in a vacuum and then solvated in a rhomboidal dodecahedron of side 3.996 nm containing 1500 TIP3P water molecules. The calculated vacuum molecular energy surfaces for the α(1→2) and α(1→3) linkages as a function of glycosidic torsional angles are displayed within Figures 1, 2, and 6, using energy contours at 1 kcal/mol intervals above the predicted minimum. The conformation of the glycosidic linkage is characterized using the two angles ϕ and ψ, which correspond to the two torsional angles (H1−C1−O×−C×) and (C1−O×−C×−H×), respectively, where × is dependent on the linkage. These molecular energy surfaces were calculated by rotating the relevant disaccharides through their ϕ and ψ angles in a stepwise fashion, at 5° intervals. At each point the disaccharides were thoroughly energy minimized, holding the glycosidic angles fixed. Following minimization, the total energy was recorded for that conformation, using a dielectric constant of 80.0 in electrostatic calculations.

At α(1→3) linkages, two distinct minimum energy regions were observed, one with $\psi = 0°$ and the other with $\psi = -160°$. In Figures 1 and 2 the two alternative energy minima predicted for the α(1→3) linkages are labeled region (A) and region (B), respectively. Therefore, two simulations were performed. In the *first*, all of the α(1→3) linkages were started in region (A), and in the *second*, all of the α(1→3) linkages were started in region (B). During each simulation the covalent hydrogen bond lengths were kept constant with the SHAKE algorithm and a 2 fs integration step was used. Long-range electrostatic interactions were treated by using periodic-boundary conditions and a nonbonded interaction cutoff of 1.2 nm. Each simulation was continued for a total of 20 ns, or 10 million steps, at a constant temperature of 300 K by weak coupling to a heat-bath. Coordinates were recorded every 0.2 ps for analysis purposes.

Theoretical Section

Predicting Relaxation Parameters. Equation 1

$$\Gamma_{ij} = \begin{cases} \frac{1}{4}\sum_{k\neq i}^{N} d_{ik}^2\{J(\omega_i - \omega_k) + 3J(\omega_i) + 6J(\omega_i + \omega_k)\} & \text{for } i = j \\ \frac{1}{4} d_{ik}^2\{6J(\omega_i + \omega_k) - J(\omega_i - \omega_k)\} & \text{for } i \neq j \end{cases}$$

$$d_{ik}^2 = \left(\frac{\mu_0}{4\pi}\right)^2 \gamma_i^2 \gamma_k^2 \hbar^2 \langle r_{ik}^{-6} \rangle \qquad (1)$$

shows the expression for the self- and cross-relaxation rates required to evaluate Γ_{ij}, the relaxation matrix.[30] In this equation, γ_i represents the gyromagnetic raito, μ_0 is the permeability of the vacuum, r_{ik} is the distance between the two nuclei, and $J(\omega)$ is the spectral density function for dipolar interactions. All NOESY predictions were based on solution of the set of simultaneous equations involving Γ at a particular mixing time by matrix diagonalization.[34] The pentasaccharide contains 35 nonexchangeable protons, and thus Γ was a 35 × 35 matrix.

Two methods were used to obtain $J(\omega)$. The first was based on the Lipari−Szabo model-free approach,[35] given by eq 2. In this model each relaxing pair has an overall tumbling correlation time τ_c, an internal motion correlation time τ_e, and an order parameter S^2. Order parameters (S^2) and internal motion correlation times (τ_e) were estimated from the simulation by calculating angular correlation functions *c(t)* in the molecular fixed frame, eq 3, where $\hat{\boldsymbol{\mu}}$ is the normalized internuclear vector.

$$J(\omega) = \frac{2}{5}\left(\frac{S^2\tau_c}{1+\omega^2\tau_c^2} + \frac{(1-S^2)\tau}{1+\omega^2\tau^2}\right)$$

$$\tau^{-1} = \tau_c^{-1} + \tau_e^{-1} \qquad (2)$$

$$c(t) = \frac{1}{5}\langle P_2(\hat{\boldsymbol{\mu}}(0)\cdot\hat{\boldsymbol{\mu}}(t))\rangle$$

$$P_2(x) = \frac{1}{2}(3x^2 - 1) \qquad (3)$$

The molecular fixed frame was defined by transforming all coordinate sets such that they had the least mass-weighted separation between them. With this method it was not possible to totally separate internal from overall motion, and only the early parts of the internal motion correlation functions were fitted to the internal correlation function predicted from the

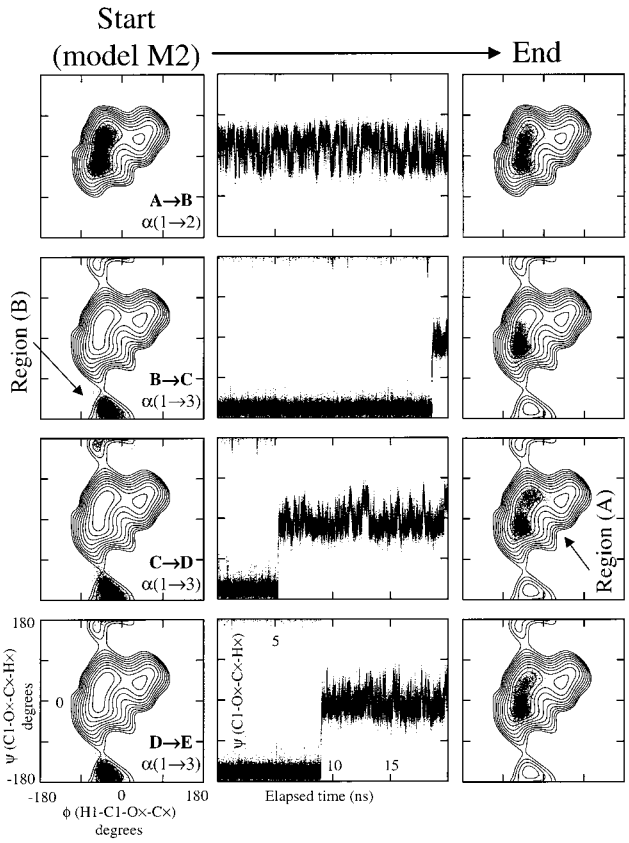

Figure 2. Exploration of the glycosidic linkages during a 20 ns simulation where all of the α(1→3) linkages were started in low-energy conformational region (B). On the left are scatter diagrams showing the exploration of the (ϕ,ψ) angles during the first 5 ns of the simulation, similar to Figure 1. This subset of the simulation in which the α(1→3) linkages are in region (B) represents dynamic model M2. In the center the exploration of the ψ angles during the simulation are plotted, showing how the α(1→3) linkages relax from region (B) to region (A) of the molecular energy surface. On the right scatter diagrams are plotted using the last 2 ns of the simulation showing the final structural ensemble, which has converged to the same region as the simulation shown in Figure 1.

(32) Brooks, B. R.; Bruccoleri, R. E.; Olafson, B. D.; States, D. J.; Swaminathan, S.; Karplus, M. *J. Comput. Chem.* **1983**, *4*, 187−217.
(33) Woods, R. J.; Dwek, R. A.; Edge, C. J.; Fraser-Reid, B. *J. Phys. Chem.* **1995**, *99*, 3832−3846.
(34) Forster, M. J. *J. Comput. Chem.* **1991**, *12*, 292−300.
(35) Lipari, G.; Szabo, A. *J. Am. Chem. Soc.* **1982**, *104*, 4546−4559.

model free approach. The appropriate value for τ_c was calculated by fitting the predicted NOESY intensities to NOESY intensities measured from proton pairs in fixed relative geometries. Proton pairs covalently bonded to the same sugar ring were considered to be in a fixed relative geometry.

Second, the spectral density function was calculated explicitly from the simulation, by evaluating the angular correlation function, eq 3, and then performing a Fourier transform, eq 4. The NOESY intensities were again predicted by evaluating the matrix in eq 1 and then diagonalizing.

$$J(\omega) = 2\int_0^\infty c(t)\cos(\omega t)\,\mathrm{d}t \tag{4}$$

The ^{13}C T_1 values were predicted using the same method. The spectral density function $J(\omega)$ was evaluated using eq 3 and then Fourier transformed as in eq 4. The self-relaxation rate was calculated using eq 1, by assuming that the C−H nuclei relax as a two-spin system.[30] In this expression the C−H bond length was taken as 0.111 nm.[36]

Predicting Residual Dipolar Couplings. For each individual frame in the simulation (output every 0.2 ps of dynamics), it was assumed that the aligning effect of the phages was symmetrical along the principal alignment axis $\mathbf{m}_a$ of the atomic distribution,[37] and asymmetrical along the other two axes, $\mathbf{m_x}$ and $\mathbf{m_y}$. To represent the shape of the atomic distribution, we used the molecular inertia tensor evaluated at every point in the simulation. It can be shown that the eigenvectors of M_{ij}, eq 5, are coincident with those of the inertia tensor and $\mathbf{m}_a$ is the eigenvector lying along the long axis of the molecule. In eq 5, the scalar M is the total molecular mass, and $m^{(r)}$ and $\mathbf{x}^{(r)}$ are the mass and position of the rth atom.

$$M_{ij} = \frac{1}{M}\sum_r m^{(r)} x_i^{(r)} x_j^{(r)} \tag{5}$$

If $\mathbf{m_x}$ and $\mathbf{m_y}$ are the other eigenvectors of M_{ij} and λ_a, λ_x, and λ_y are the corresponding eigenvalues, it was found that there was no preferred direction for $\mathbf{m_x}$ and $\mathbf{m_y}$ within this molecule. This arose because $\lambda_x \approx \lambda_y$ and hence the molecule possesses cylindrical symmetry to a good approximation in all conformations. Further, it was found that $\lambda_a \gg \lambda_x, \lambda_y$, and thus there was no need to consider an asymmetric component in the alignment tensor.[38] In this case all net alignment is in the direction of $\mathbf{m_a}$ to a good approximation. This simplifies calculation of the residual dipolar couplings somewhat since a tensorial representation of alignment is not necessary. However, it should be pointed out this is not general to all molecular shapes and thus must be checked on a case-by-case basis. If θ is the instantaneous angle between the alignment axis $\mathbf{m_a}$ and $\hat{\mathbf{r}}_{ij}$, the unit vector connecting the two nuclei at time t, then $\cos\theta = \mathbf{m_a}\cdot\hat{\mathbf{r}}_{ij}$. Standard formulas can then be used to relate $\cos\theta$ to the residual dipolar coupling at time t. In eq 6 this has been averaged over time to obtain the experimentally observed quantity $\langle D_{ij}\rangle$. A similar approach has been used previously to analyze a lacto-N-neotetraose tetrasaccharide.[39]

$$\langle D_{ij}\rangle = -\kappa^2\langle r_{ij}^{-3}\{3(\mathbf{m}_a\cdot\hat{\mathbf{r}}_{ij})^2 - 1\}\rangle \tag{6}$$

However, calculation of $\langle D_{ij}\rangle$ can only be obtained from the simulation subject to a positive constant of proportionality, κ^2, which depends on many experimental parameters, e.g., concentration of phages. Least-squares fitting between the experimental data and theoretical predictions was used to determine the value of κ^2. Since both heteronuclear (C−H) and homonuclear (H−H) residual dipolar couplings were measured under the same sample conditions, then it is apparent that eq 7 holds, where κ_{HC}^2 and κ_{HH}^2 are the constants of proportionality in the hetero- and homonuclear cases, respectively, and γ represents the nuclear gyromagnetic ratio. Thus, the constants of proportionality for the two sets of measurements are related and only one needs to be fitted.

$$\frac{\kappa_{HH}^2}{\kappa_{HC}^2} = \frac{\gamma_H}{\gamma_C} \tag{7}$$

Results and Discussion

A schematic picture of the pentamannan chemical structure is shown in Figure 1, showing the alphabetical labeling of the monosaccharides used throughout the text.

Dynamical Predictions from Molecular Dynamics Simulations. Calculation of the molecular energy surface for an α(1→3) linked mannose disaccharide as a function of the glycosidic torsional angles indicated that there are two distinct minimum energy regions, as previously documented.[18,40,41] One region corresponds to that around $(\phi,\psi) = (-50,0)$, see Materials and Methods for definitions, and will subsequently be referred to as region (A). The other region corresponds to $(\phi,\psi) = (-30,-160)$, which will subsequently be referred to as region (B), see Figure 1. For the α(1→2) linkage, only one major low-energy region was predicted, as found in previous studies based on vacuum molecular modeling and NMR relaxation.[42]

Two 20 ns molecular dynamics simulation were performed each with inclusion of 1500 water molecules. The *first* simulation was started in a conformation with all the α(1→3) linkages in region (A), and subsequently the molecule remained in region (A), as shown in Figure 1. This molecular ensemble will be referred to as dynamic model M1. The *second* simulation was started with all of these linkages in region (B). Following 20 ns of molecular dynamics, it was noted that in this second simulation all of the α(1→3) linkages had made the transition from region (B) to region (A), and this is represented in Figure 2. The portion of this simulation where all of the α(1→3) linkages are in region (B) will be called dynamic model M2. Thus, solvated molecular dynamics simulations predict that region (A) is the preferred region for all of the α(1→3) linkages in this structure. This prediction was compared against the experimental data, as described below.

Prediction of NOESY Experimental Data. The initial question was if molecular dynamics simulations of a flexible molecules were capable of predicting NOESY enhancements. Well-resolved peaks in the NOESY spectra were integrated at all three mixing times using the Pronto software,[43] and inter-residue NOEs were obtained. The values for specific intensities

(36) Söderman, P.; Widmalm, G. *Magn. Reson. Chem.* **1999**, *37*, 586−590.
(37) Zweckstetter, M.; Bax, A. *J. Am. Chem. Soc.* **2000**, *122*, 3791−3792.
(38) Kiddle, G. R.; Homans, S. W. *FEBS Lett.* **1998**, *436*, 128−130.
(39) Rundlöf, T.; Landersjö, C.; Lycknert, K.; Maliniak, A.; Widmalm, G. *Magn. Reson. Chem.* **1998**, 773−776.
(40) Dowd, M. K.; French, A. D. *J. Carbohydr. Chem.* **1995**, *14*, 589−600.
(41) Homans, S. W.; Pastore, A.; Dwek, R. A.; Rademacher, T. W. *Biochemistry* **1987**, *26*, 6649−6655.
(42) Helander, A.; Kenne, L.; Oscarson, S.; Peters, T.; Brisson, J.-R. *Carbohydr. Res.* **1992**, *230*, 299−318.
(43) Kjær, M.; Andersen, K. V.; Poulsen, F. M. *Methods Enzymol.* **1994**, *239*, 288−307.

Table 2. Experimental NOESY Intensities for Three Different Mixing Times, Shown in Column Labeled "exp" [a]

	mixing time (ms)								
	150			300			450		
NOESY cross-peak	exp	model M1	model M2	exp	model M1	model M2	exp	model M1	model M2
B H1−A H2	1.1	1.9	2.0	1.9	3.4	3.5	2.6	4.5	4.8
C H1−B H3	1.3	1.6	0.1	2.3	2.9	0.2	3.2	3.9	0.3
D H1−C H3	1.8	1.7	0.1	3.4	2.9	0.2	4.6	3.9	0.3
E H1−D H3	1.5	1.7	0.1	2.6	3.0	0.2	3.5	4.1	0.3
A H1−B H5	0.4	0.9	1.1	0.7	1.6	2.1	1.1	2.1	2.8
B H2−C H5[b]	0.7	0.9	0.0	1.4	1.5	0.0	1.7	2.1	0.0
C H2−D H5[b]	0.7	0.8	0.0	1.4	1.7	0.0	1.7	2.2	0.0
B H1−B H2	0.9	0.9	0.9	1.5	1.6	1.6	2.2	2.2	2.2
C H1−C H2[b]	1.1	0.9	0.9	2.0	1.6	1.6	2.7	2.2	2.2
D H1−D H2[b]	1.1	0.9	0.9	2.0	1.6	1.6	2.7	2.2	2.2
E H1−E H2	0.6	0.9	0.9	1.1	1.7	1.7	1.5	2.4	2.4

[a] The values were normalized as a percentage of the diagonal peak intensity at zero mixing time, and an average value was calculated from the cross-peak intensities above and below the diagonal. Predictions were calculated using dynamic model M1 (Figure 1) and dynamic model M2 (Figure 2) by evaluation of the full relaxation-matrix (see Theoretical Section). The predictions are shown alongside the experimental data. In predictions the Lipari and Szabo model-free approach was used (see text), with the order parameter (S^2) set to 1.0, to estimate the spectral density $J(\omega)$. The overall tumbling time τ_c was calculated to be 440 ps for model M1 and 450 ps for model M2. [b]These NOESY intensities were biased toward values above the diagonal due to overlap.

at three mixing times are detailed in Table 2. The expected NOESY enhancements were predicted from two molecular dynamics trajectories: one trajectory with α(1→3) linkages fully in region (A), dynamic model M1 discussed above, and the other in region (B), dynamic model M2. All predictions were made using a full relaxation matrix analysis method, to take into account multiple relaxation pathways (see Theoretical Section). However, prediction of the relaxation matrix Γ, eq 1, requires the spectral density functions $J(\omega)$ to be estimated theoretically for relaxing nuclear pairs. Attempts were made to estimate $J(\omega)$ from the simulations using model-free and model-dependent methods, as described below.

In the first instance, a Lipari−Szabo type of model-free approach[35] was used to estimate the spectral densities, as shown in eq 2. A preliminary prediction was obtained by setting $S^2 = 1.0$ (no internal motion). The relaxation matrices for simulations in both region (A), dynamic model M1, and region (B), dynamic model M2, were calculated from molecular dynamics simulation data, as described above and in Figures 1 and 2. This involved use of eq 1 and averaged (r^{-6}) distances from the simulation (see Theoretical Section). By varying τ_c the best fit was obtained between the NOESY intensities predicted from the relaxation matrix and the experimental data for protons in fixed relative geometries within sugar rings. The predictions using dynamic models M1 and M2 employed τ_c values of 440 ps and 450 ps, respectively, by least-squares fitting to a subset of the experimental data (see Materials and Methods). The resultant predicted intensities are shown in Table 2.

Comparing all NOESY predictions against the experimental data shows that the trajectory from region (B), dynamic model M2, makes poor predictions of the experimental data. However, predictions based on the simulation in region (A), dynamic model M1, are relatively close to the experimental data, even using this coarse model which neglects internal motion. Further, the predictions based on region (A) could not be improved by using a linear combination of region (A) and (B). Hence on the basis of NOESY data there is no reason to propose that the α(1→3) linkages populate anything other than region (A).

Whether the inclusion of internal motion to the relaxing proton pairs could improve the fit of the experimental data to dynamic model M1 was investigated. One assumption of the Lipari−Szabo model is that internal motions can be separated from the overall tumbling.[35] However, in our case the overall tumbling is not predicted to occur as a rigid body. Hence the deconvolution of motion into an overall tumbling correlation time (τ_c) and internal-motion parameters (S^2,τ_e) did not make strict sense for this oligosaccharide, which is a known problem for small molecules.[36,44] For the pentamannan, the internal-motion parameters (S^2,τ_e) for proton pairs were estimated by fitting to an angular correlation function in a pseudo-molecular frame (see Theoretical Section). Estimated internal-motion parameters for well-resolved proton pairs in the NOESY spectra are given in Table 3. The trend was for order parameters to be higher at the center of the molecule than at the ends. Again, τ_c was estimated by fitting of the predicted NOESY intensities to the experimental data for protons in fixed relative geometries. Use of the Lipari−Szabo model, with order parameters calculated from the simulation in region (A), allowed predictions of the NOESY intensities to be in closer agreement with experiment than when order parameters were set to 1.0 (compare Tables 2 and 3). In this case a value of $\tau_c = 520$ ps was

Table 3. Experimental NOESY Intensities at a Mixing Time of 300 ms (see Table 2) Compared against Theoretical Predictions Using Dynamic Model M1 (see Figure 1)[a]

NOESY cross-peak	simulation S^2	τ_e (ps)	predctn (% diagonal)	exptl (% diagonal)
B H1−A H2	0.57	35	2.0	1.9
C H1−B H3	0.76	36	2.6	2.3
D H1−C H3	0.76	33	2.7	3.4
E H1−D H3	0.70	41	1.8	2.6
A H1−B H5	0.53	35	0.8	0.7
B H2−C H5	0.72	35	1.3	1.4
C H2−D H5	0.72	29	1.4	1.4
B H1−B H2	0.87	26	1.9	1.5
C H1−C H2	0.90	30	1.9	2.0
D H1−D H2	0.84	28	1.8	2.0
E H1−E H2	0.57	33	1.0	1.1

[a] The predictions were made by solving a full relaxation-matrix (see Theoretical Section). In these predictions the Lipari and Szabo model-free approach was used (see text) with order parameters, to estimate the spectral density $J(\omega)$. The values for S^2 and τ_e were estimated by fitting them to the first 150 ps of a molecular frame angular correlation function (see Materials and Methods). A value of τ_c equal to 520 ps was fitted to the experimental data. Use of order parameters allowed better agreement to the experimental data than without (compare Table 2).

(44) Hricovíni, M.; Shah, R. N.; Carver, J. P. *Biochemistry* **1992**, *31*, 10018−10023.

calculated by fitting the predictions to a subset of the experimental data (see Materials and Methods). Calculation of the NOESY intensities based on an anisotropic cyclinder model[45] could not improve the predictions given in Table 3 against the experimental observations, even though it is evident from the shape of the pentasaccharide that the molecule does not tumble isotropically.

On the basis of the NOESY data and predictions from our simulations, there is no evidence for significant populations of region (B) at the α(1→3) linkages of this molecule in aqueous solution. Thus, it is inferred that all of the α(1→3) linkages populate region (A). This agrees well with the results from our molecular dynamics simulation. Our second simulation indicated that when the α(1→3) linkages are in region (B), they are not in equilibrium and they quickly make the transition to region (A). This proposition is also in agreement with previous studies which used NOESY data,[41] potential energy calculations, and crystal structures.[46]

Rather than using the Lipari−Szabo model, calculation of the spectral densities for dipolar relaxation directly from the simulation was attempted, by Fourier transformation of the angular correlation functions, see eqs 3 and 4 in the Theoretical Section. However, the required precision on the difference between $J(0)$ and $6J(2\omega_H)$ could not be obtained to provide prediction of the cross-relaxation rate, eq 1. A direct prediction of the cross-relaxation rates for use in NOESY prediction necessitates longer simulations. Therefore, it is proposed that NOESY data cannot be used as an exact quantitative test of oligosaccharide simulations on the nanosecond time scale.

Prediction of ^{13}C Relaxation Data. Carbon relaxation was measured to test if the simulation could correctly reproduce overall hydrodynamic behavior and internal motions.[47] Longitudinal relaxation (T_1) of ^{13}C nuclei were measured using a 2D INEPT−inversion−recovery−HSQC NMR experiment, as described in the Materials and Methods section. Cross-peak separation in the 2D spectrum allowed the relaxation of nine carbon nuclei to be measured. If the relaxation rate is assumed to be predominantly dipolar and only to the adjacent proton, then the relaxation rate in this two-spin system should be purely exponential,[30] which can be shown from eq 1. Therefore, the ^{13}C T_1 values calculated using a three-parameter fit to the experimental data are given in Table 4.

The spectral density function *J(ω)* was calculated explicitly from the first simulated trajectory, dynamic model M1, in which all of the α(1→3) linkages were in region (A). That is by Fourier transformation of the angular correlation function using eqs 3 and 4. In this case no subtraction of *J*-terms was required and an acceptable error on the transformed correlation function was obtained, unlike in predictions of the NOESY data. By transforming subsections of the trajectory, it was estimated that the spectral density could be obtained with ≈10% error. This allowed direct calculation of the relevant *J*-terms for eq 1 from the simulation. The T_1 values calculated by this method are shown in Table 4. It should be pointed out, however, that the NMR measurements were made in D_2O solution and the simulations performed in H_2O. Although it has been established a small dependence of the conformation of oligosaccharides on solvent exists,[48] it is known that the viscosity of the D_2O solution is greater than that of H_2O at 300 K.[49] The effect of viscosity on overall tumbling, and hence on the calculation of *J*-terms, is predicted to be smaller than the error by which we could estimate them from the simulation. For this reason we disregarded the difference in solvent condition. Therefore, it is proposed that, within error, our predictions of carbon relaxation obtained from molecular dynamics simulations are in agreement with the experimentally measured values.

Table 4. Measured ^{13}C T_1 Values Based on a Three-Parameter Fit to the Experimental Data[a]

residue (Figure 1)	carbon	without phage ^{13}C T_1 (s)	with phage ^{13}C T_1 (s)	predicted ^{13}C T_1 (s)
A	C1	0.40 ± 0.01	0.59 ± 0.15	0.46 ± 0.05
A	C3	0.41 ± 0.01	0.53 ± 0.13	0.50 ± 0.05
A	C3	0.30 ± 0.01	0.40 ± 0.13	0.38 ± 0.04
A	C4	0.43 ± 0.03	0.43 ± 0.13	0.38 ± 0.04
B	C1	0.39 ± 0.01	0.29 ± 0.06	0.41 ± 0.04
B	C3	0.44 ± 0.03	0.33 ± 0.11	0.42 ± 0.04
E	C2	0.60 ± 0.02	0.44 ± 0.11	0.63 ± 0.06
E	C3	0.36 ± 0.02	0.34 ± 0.09	0.55 ± 0.06
E	C4	0.40 ± 0.01	0.55 ± 0.17	0.54 ± 0.05

[a] Errors are quoted to 1 standard deviation. When phages were added, the signal-to-noise ratio obtained in the recorded HSQC spectra was reduced by a factor of 10, and this resulted in increased errors in T_1 values. The predictions were based on explicit calculation of the spectral density function $J(\omega)$ from the molecular dynamics simulation, by Fourier transformation of an angular correlation function. In this calculation the C−H bond length was assumed to be 0.111 nm.

Prediction of Residual Dipolar Coupling. Recent studies have shown that residual dipolar couplings provide valuable information about oligosaccharides conformation[50] but have favored their interpretation in terms of well-defined single structures.[51] Therefore, a question arises as to whether for this fully α-linked carbohydrate a dynamic ensemble can satisfy both relaxation and residual dipolar coupling observations simultaneously. Thus, the pentasaccharide was mixed with phages and residual dipolar couplings were measured as described in the Materials and Methods section. No chemical shift changes were observed, indicative of the overall sugar conformations not being altered by the presence of phages. The proton spin−spin and spin−lattice relaxation times were measured where possible with and without phages, as described in the methods section, and the data are presented in Table 1. There were slight observed differences in the proton T_1 and T_2 values, obtained with and without phages. These effects were attributed to differences in the average solvent environment and the increased line widths induced by the presence of phages. For a more accurate representation of changes in overall tumbling and internal dynamics, the ^{13}C T_1 relaxation measurements were repeated in the presence of phages. These data are shown in Table 4. With phages present, a reduced signal-to-noise ratio was obtained, and the line broadening made measuring peak heights more problematic, thus the errors on the ^{13}C T_1 values in phage were increased somewhat. However, no significant changes were observed in the ^{13}C T_1 values when phages were added to the sample. These data provide good evidence that the oligosaccharide has similar hydrodynamic behavior with and without phages.

The S^{3}CT HSQC and S^{3}CT TOCSY spectra, recorded with and without phage, allowed the measurement of both C−H and

(45) Rundlöf, T.; Venable, R. M.; Pastor, R. W.; Kowalewski, J.; Widmalm, G. *J. Am. Chem. Soc.* **1999**, *121*, 11847−11854.
(46) Warin, V.; Baert, F.; Fouret, R.; Strecker, G.; Spik, G.; Fournet, B.; Montreuil, J. *Carbohydr. Res.* **1979**, *76*, 11−22.
(47) Doddrell, D.; Glushko, V.; Allerhand, A. *J. Chem. Phys.* **1972**, *56*, 3683−3689.
(48) Cagas, P.; Bush, C. A. *Biopolymers* **1990**, *30*, 1123−1138.
(49) Cavanagh, J.; Fairbrother, W. J.; Palmer, A. G.; Skelton, N. J. *Protein NMR spectroscopy: principles and practice*; Academic Press: 1996.
(50) Martin-Pastor, M.; Bush, C. A. *Carbohydr. Res.* **2000**, *323*, 147−155.
(51) Martin-Pastor, M.; Bush, C. A. *Biochemistry* **2000**, *39*, 4674−4683.

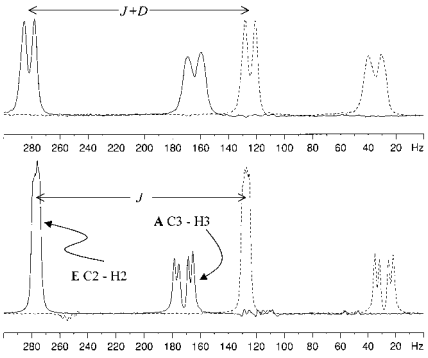

Figure 3. Superimposed ω_2-traces of the two S^{3}CT subspectra for measurement of one-bond ^{13}C−^{1}H coupling constants. The bottom traces are from the two edited subspectra before the addition of phages. The top traces are from the two edited subspectra obtained after the addition of phages, in which the line broadening induced by the phages can be clearly seen. In this diagram the α and β spin states are drawn with dashed and solid lines, repectively.

Table 5. Experimentally Measured Residual Dipolar Couplings (in Hz) Obtained from Measurements of the Pentamannan Oligosaccharide with a Phage Cosolute[a]

assignment	exptl data	static models			dynamic models	
		S1	S2	S3	M1	M2
A C1−H1	4.5	2.9	9.3	7.6	6.1	5.0
A C2−H2	6.9	9.7	1.0	−17.4	6.0	4.0
A C3−H3	−14.3	−13.7	7.6	10.0	−13.3	−6.0
A C4−H4	−13.9	−12.2	6.6	9.6	−13.7	−6.4
A C5−H5	−11.9	−12.3	8.4	9.5	−14.0	−6.5
B C1−H1	9.6	8.4	9.9	9.5	5.0	4.9
B C3−H3	3.4	3.1	5.9	−1.7	6.1	3.5
C C1−H1	4.4	3.8	6.8	−3.0	4.5	3.2
D C1−H1	9.4	9.1	2.3	−5.7	6.0	3.7
E C1−H1	3.7	4.6	8.1	−17.7	3.5	5.2
E C2−H2	8.0	8.4	9.8	−2.5	8.0	−2.6
E C3−H3	4.5	2.9	−9.6	9.5	5.2	−7.0
E C4−H4	3.1	2.7	−14.5	9.9	4.4	−7.3
A H1−H2	2.8	3.1	−2.1	−1.6	2.0	0.7
A H4−H5	−2.3	−2.3	−0.5	0.8	−2.4	−1.2
B H1−H2	−2.5	−1.4	−2.6	−0.8	−2.9	−1.3
E H1−H2	−2.0	−1.5	2.3	3.2	−2.2	1.2
E H2−H3	3.3	3.2	2.6	−6.0	2.6	1.4
E H3−H4	1.1	1.1	−0.2	1.4	1.4	−1.2
E H4−H5	−1.1	−2.1	−3.4	1.8	−1.2	−0.7
E H2−H4	0.5	0.4	0.7	−0.8	0.6	−0.3
A H1−B H1	−0.8	−3.4	−6.0	−5.0	−0.8	−0.5

[a] Alongside this are a series of predictions from different models. The columns labeled S1, S2, and S3 result from various static structures, which are explained in the text and Figures 5 and 6. The columns labeled M1 and M2 are the result of an average of two respective dynamic ensembles produced by molecular dynamics simulation. The models M1 and M2 are described in the text and Figures 1 and 2.

H−H residual dipolar couplings. The use of the S^{3}CT sequence, as opposed to the nondecoupled HSQC sequence,[51] allows the determination of residual dipolar couplings for resonances in crowded regions of the spectra, by separation into two subspectra. Figure 3 shows sample ω_2-traces from the S^{3}CT HSQC spectra, recorded before and after inclusion of phages. It shows the line broadening induced by unresolved weak residual dipolar couplings. The experimentally measured residual dipolar couplings are given in Table 5.

Residual dipolar couplings were calculated as a function of time from the two molecular dynamics trajectories, dynamic models M1 and M2, as described in the Theoretical Section. The values were then averaged over the trajectory, or relevant subsection of it, and compared with the experimental data. The predictions from these dynamic trajectories are presented in

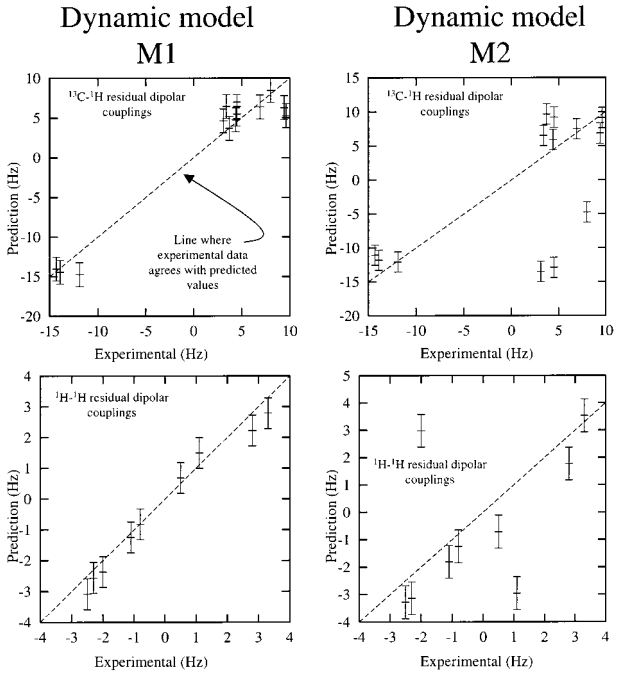

Figure 4. Correlation between experimentally measured residual dipolar couplings and the theoretical prediction for the two dynamic models of the oligosaccharide. The two graphs on the left show predictions based on dynamic model M1, where all of the α(1→3) linkages are in conformational region (A), see Figure 1. The two graphs on the right show predictions based on dynamic model M2, where all of the α(1→3) linkages are in conformational region (B), see Figure 2.

Table 5, columns M1 and M2, and are plotted against the experimental data in Figure 4. Again it was observed that the trajectory with α(1→3) linkages in region (A), dynamic model M1, fitted well with the experimental data. However, the trajectory with the α(1→3) linkages in region (B), dynamic model M2, did not. Predictions, using eq 6, based on dynamic model M1, were scaled with a constant of $\kappa^2 = 27.36$ in the heteronuclear case and $\kappa^2 = 104.7$ in the homonuclear case. Use of eq 7 gives $\gamma_H/\gamma_C = 3.8$, which is close to the correct value of 3.977.

In the second trajectory, the three α(1→3) linkages made transitions from region (B) to region (A) at separate times. This is shown in Figure 2, which details the value of the ψ glycosidic linkages at the three α(1→3) linkages as a function of time. To further the argument given above, no observed conformation of the molecule with α(1→3) linkages in a mixture of region (A) and region (B) was found to be consistent with the experimental data. Therefore, it is inferred from both NOESY and residual dipolar coupling data that all of the α(1→3) linkages exist in the region corresponding to region (A) in aqueous solution. Hence both experiment and molecular dynamics simulation agree on the highly populated region for this pentamannan. It is noted from Figure 2 that the length of time required to traverse the barrier from (B) to (A) is of the order 1−10 ns, and no transitions were ever observed from (A) back to (B). This time was much longer than that expected from the adiabatic surface of the molecule; therefore it is proposed that the main restriction to conformational change was due to solvent rearrangement.

Single Structure or Dynamic Ensemble? Use of molecular dynamics simulations allowed predictions of residual dipolar couplings to be made without invoking a motional order parameter.[52] However, it is perhaps not surprising that there exists a well-defined single-structure in the ensemble which can

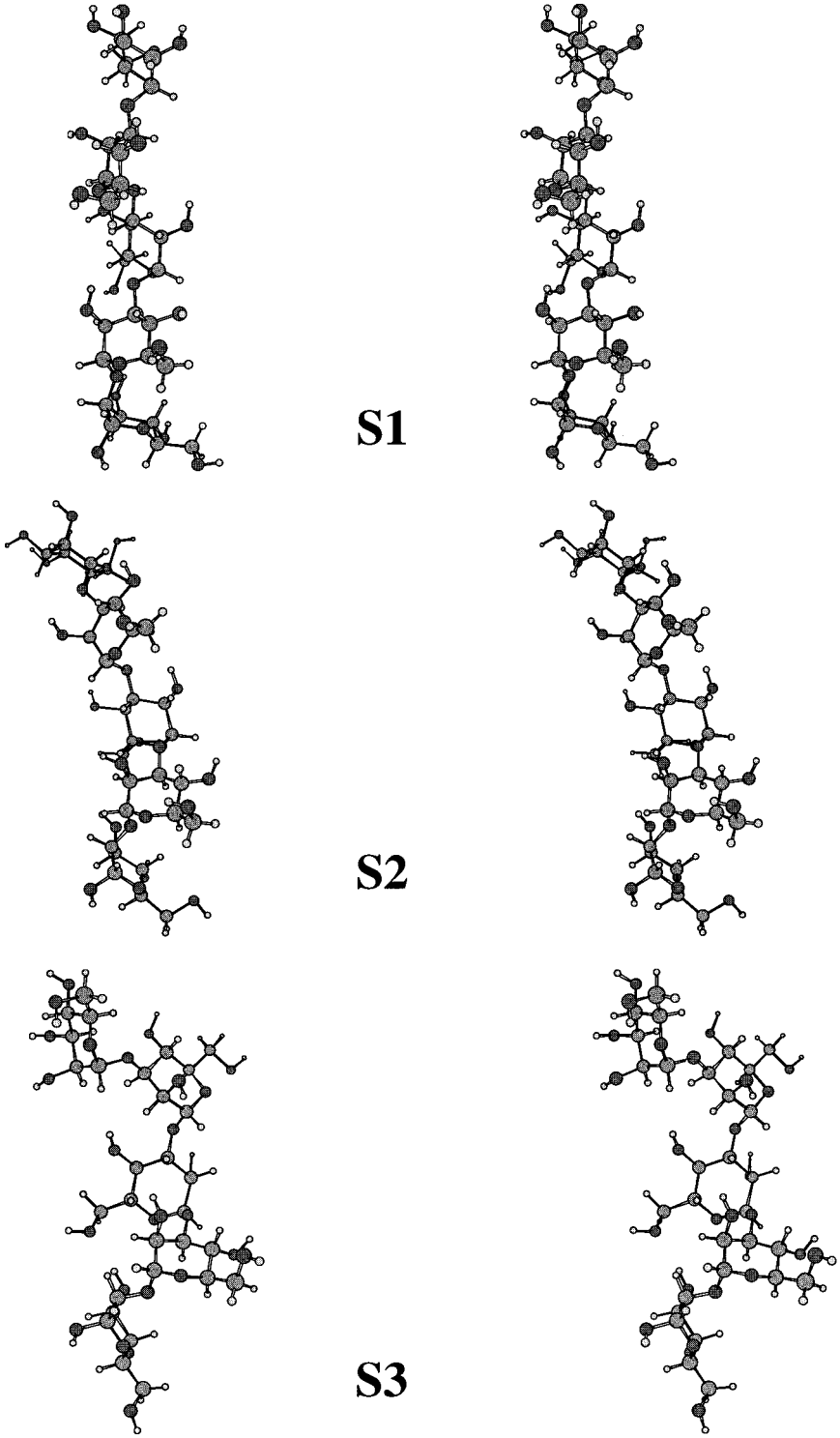

Figure 5. Stereoviews of the static structures S1, S2, and S3 used for prediction of residual dipolar couplings. The conformation of the glycosidic angles is shown in Figure 6. Structure S1 gave the closest agreement with the residual dipolar couplings. However, structures S2 and S3 do not agree well with the experimental data, even though structure S2 is close in conformational space to structure S1 (see Figure 6).

be used to predict the residual dipolar couplings. This structure (called S1) is shown in Figure 5 and the predicted residual dipolar couplings in Table 5. In this case the (ϕ,ψ) angles of the linkages were (−30,47), (−39,−29), (−52,−20), and (−46,12), and hence all of the α(1→3) linkages are in region (A), see Figure 6. The linkages are listed in the order α(1→2) between sugar A and B, α(1→3) between B and C, α(1→3) between C and D, and α(1→3) between D and E.

As a test of the robustness of a single structure in predicting the residual dipolar couplings, we asked if there were other valid structures in which all of the α(1→3) linkages were in region (A) for which the agreement with the experimental data was not so good. Therefore, the linkages were perturbed to a structure close to S1 with the following glycosidic angles: (−17,40), (−66,16), (−28,−9), (−63,-31), see Figure 6. This produced a second single structure (S2) which was also populated during the simulation, to an extent not dissimilar to S1, and with all of the α(1→3) linkages still resident in region (A). This single

(52) Landersjö, C.; Höög, C.; Maliniak, A.; Widmalm, G. *J. Phys. Chem. B* **2000**, *104*, 5618−5624.

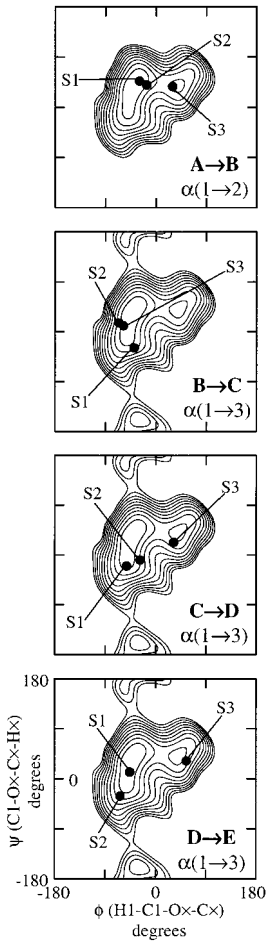

Figure 6. The conformation of the pentamannan glycosidic angles (ϕ,ψ) in the three selected static conformations: S1, S2, and S3. These graphs have the same format as those in Figures 1 and 2. Structure S1 gave the closest agreement with the residual dipolar couplings. Structures S2 and S3 have all α(1→3) linkages in region (A) but do not agree well with the experimental data. Notice how close structure S2 is to S1 in conformational space.

structure results in a prediction of the residual dipolar couplings shown in Table 5, and can be viewed in Figure 5. However, these predictions are far from the experimentally observed values and would not be considered to be in agreement. As an example of another allowable single structure, the conformation S3 was chosen, which has all the α(1→3) linkages in region (A) at (29,37), (−58,11), (32,23), (55,32), see Figure 6. However, predictions based on this conformation alone, which was populated in the our molecular dynamics simulation, cannot possibly agree with the experimental data. Its three-dimensional structure is drawn in Figure 5, and the predictions from it are shown in Table 5. Therefore, all of the single structures S1, S2, and S3 are valid structures and were populated in our molecular dynamics simulation. It is not clear, however, why one should choose single structure S1 against S2 or S3 *a priori*, other than for the fact that it fits the residual dipolar coupling data. Hence, the interpretation of residual dipolar couplings as single structures is rather arbitrary.

Although the experimental residual dipolar coupling data is in agreement with both a dynamic ensemble and an arbitrary single structure, a dynamic ensemble is required to predict the experimental relaxation data. This is because relaxation processes result not only from the shape of the molecule but also internal motion and overall tumbling of the molecule. Therefore, it is proposed that caution should be exercised in the interpretation of residual dipolar couplings, and in particular the presence of well-defined single structures should not be inferred for flexible molecules.

Other studies, not using residual dipolar couplings, have also emphasized that single conformations are not sufficient to agree with experimental data, in cellobiose, for example.[53] This is particularly evident when the same molecule is studied by different experimental techniques. In a set of recent studies, similar complex carbohydrates were investigated separately by NMR relaxation[45] and by residual dipolar couplings.[50,51] Relaxation studies concluded the presence of significant internal motion. However, the residual dipolar coupling data could be interpreted in terms of a single structure. The argument provided here allows these two seemingly contradictory conclusions to be reconciled.

The Microscopic Interpretation. The internal motion emergent from our simulations results from a combination of intramolecular interactions and interaction with water. However, to those interested in understanding molecular dynamics, it is the interaction with water that is presently providing one of the greatest challenges. Theoretical predictions of the experimental data for a small molecule, with a large coupling to water, provides evidence that the simulation is a good representation of dynamic conformation and hence the microscopic properties of aqueous solvation. Hence, after experimental testing of the trajectories it is proposed that a detailed and informative analysis of the microscopic molecular behavior can be performed.

In previous simulations the interaction of carbohydrates with water has been monitored by observing the dynamics of intramolecular hydrogen bonds,[11] which exchange with water in a way that is determined by the geometrical arrangement of substituents. Simulations that have previously been analyzed in this way have concentrated on the β-type of carbohydrate linkage, and analysis of this molecule is an extension to these observations. There was no evidence for direct intramolecular hydrogen bonds being favored in the simulation at either the α(1→2) linkage or the α(1→3) linkages, and this is simply a consequence of the geometrical arrangement of hydroxyl groups. Lack of intramolecular hydrogen bonds is consistent with the observed internal flexibility of the oligosaccharide. Additionally, no evidence was found for intramolecular hydrogen bonds between noncontiguous residues, as has been observed in other oligosaccharides.[54]

Previous simulations of mannose-containing oligosaccharides have corroborated large conformational mobility at the α-linkages.[16,21] A similar picture has been obtained from other experiments. For example, optical rotation studies provided evidence for significant solution linkage flexibility and the population of distinct regions of the linkage (ϕ,ψ) space,[55] which agrees well with these predictions. Also, in a separate study, NOESY data from a high mannose oligosaccharide were not found to be consistent with a single conformation, indicating a high degree of internal flexibility or the presence of multiple conformations.[19] However, in that study it was concluded that in principle the considerable internal flexibility may not be translated into gross changes in structure. A similar observation was made here, and results from the geometry of the α-linkage where linkage motion results in molecular twists, rather than bends and stretches.

Studies of β-carbohydrate linkages by molecular modeling in aqueous solution have concluded a lower degree of confor-

(53) Hardy, B. J.; Sarko, A. *J. Comput. Chem.* **1993**, *14*, 848−857.
(54) Sandström, C.; Baumann, H.; Kenne, L. *J. Chem. Soc., Perkin Trans. 2* **1998**, 2385−2392.
(55) Arndt, E. R.; Stevens, E. S. *Biopolymers* **1995**, *38*, 567−571.

mational freedom[11] than that observed in α-carbohydrate linkages.[36,56] The reduced conformational freedom proposed for *β*-carbohydrate linkages is coincident with increased intramolecular hydrogen bonding.[9] In the simulations presented here we observed no intramolecular hydrogen bonds across the α-linkages. It is therefore proposed that this allows a greater amount of internal disorder at these α-linkages as compared to *β*-linkages. Further, since the twists observed at α-linkages conserve overall solvent interaction, the set of twisted conformations is expected to form a degenerate set of ground states in α-linked structures, a possible reductive explanation for the significant predicted internal motion.

Conclusions

Two aqueous simulations of a mannose pentasaccharide, each of length 20 ns, were started from distant conformations. After a period of equilibration, both simulations converged to the same flexible structure. This ensemble was found to be sufficient to predict all of the experimental data. Dynamic data in other conformations could not predict the experimental data.

In the prediction of relaxation parameters, the calculation of internal-motion order parameters was not well-defined, since the internal-motion could not be effectively separated from fast overall tumbling. It was estimated that order parameters followed a trend where they were low at the ends of the molecule and high in the middle, due to molecular flexibility. A direct approach to calculate spectral densities from explicit angular correlation functions could not be used in a relaxation matrix approach to calculation of NOESY enhancement. This was because the cross-relaxation terms require differences between spectral density terms which have large errors and indicates a limitation in using NOESY data to test molecular dynamics simulations when internal motion is convoluted with overall tumbling.

It was possible to find a single structure within the predicted ensemble in agreement with the residual dipolar coupling data. However, other valid single structures in the ensemble were not able to predict these data, and it is not clear to see why one structure should be chosen against the other. Further, by averaging the whole predicted molecular dynamics ensemble it was also possible to obtain a quantitative agreement with the residual dipolar couplings. Additionally, it was also possible to predict ^{13}C T_1 values directly from the simulation by evaluating angular correlation functions. Although a single structure was also found to be consistent with the residual dipolar coupling data, this rigid structure could not be used to explain the ^{13}C T_1 data, and no significant differences were observed in ^{13}C T_1 values when phages were added to the pentasaccharide molecule. Hence it is inferred that the simulation is reproducing both the average conformation and internal flexibility, when explicit water is present and the simulation is long enough. Therefore, it is concluded that although residual dipolar couplings can be predicted from a single structure, this is not the correct interpretation of molecular conformation and dynamics.

The predicted conformation of both the α(1→2) and α(1→3) glycosidic linkages was centered around a region observed in previous crystallography studies, although significant linkage flexibility was predicted by the simulation. No experimental evidence was found for large populations of other conformers. In this predicted dynamic conformation, the linkages did not partake in intramolecular hydrogen-bonding interactions, and the overall molecular motion was observed to be a twisting motion around the long axis of symmetry. This allowed the oligosaccharide to maintain a constant surface coupling to the external solvent water molecules.

Acknowledgment. The Danish Instrument Centre for NMR Spectroscopy of Biological Macromolecules at the Carlsberg Research Centre provided time on an 800 MHz Varian Unity Inova NMR spectrometer. We thank Paul Hanson, Mark Hansen, and Arthur Pardi for providing us with starter cultures of Pf1-phage and *Pseudomonas aeruginosa* host. We thank Prof. H. Parolis, L. A .S. Parolis, and L. Kenne for providing the sample used in this study. Thanks to Thomas Schulte-Herbrüggen for many enlightening discussions and implementation of the INEPT−inversion−relaxation pulse sequence and to Ole W. Sørensen for design of the S^3CT pulse sequences. A.A. is funded by the Wellcome Trust (grant reference number 058154). C.H.G. is funded by the Danish Technical Research Council (grant reference number 9900687).

JA0025696

(56) Blanco, J. L. J.; van Rooijen, J. J. M.; Erbel, P. J. A.; Leeflang, B. R.; Kamerling, J. P.; Vliegenthart, J. F. G. *J. Biomol. NMR* **2000**, *16*, 59−77.